

**Excitons in nitride heterostructures: From zero- to one-dimensional behavior**

D. Rosales, T. Bretagnon, and B. Gil

*CNRS-Université Montpellier 2, Laboratoire Charles Coulomb UMR 5221, F-34095 Montpellier, France  
and Université Montpellier 2, Laboratoire Charles Coulomb UMR 5221, F-34095 Montpellier, France*

A. Kahouli, J. Brault, B. Damilano, and J. Massies

*Centre de Recherche sur l'Hétéro-Épitaxie et ses Applications, CNRS, Rue Bernard Gregory, 06560 Valbonne, France*

M. V. Durnev

*Spin Optics Laboratory, St. Petersburg State University, 198504 St.-Petersburg, Russia and Ioffe Physical-Technical Institute of RAS,  
194021 St.-Petersburg, Russia*

A. V. Kavokin

*Spin Optics Laboratory, St. Petersburg State University, 198504 St.-Petersburg, Russia; Physics and Astronomy School,  
University of Southampton, Highfield, Southampton, SO171BJ, United Kingdom; and CNRS-Université Montpellier,  
Laboratoire Charles Coulomb UMR 5221, F-34095 Montpellier, France*

(Received 19 April 2013; revised manuscript received 7 July 2013; published 30 September 2013)

We report an unusual temperature dependence of exciton lifetimes in arrays of GaN nanostructures grown on semipolar (11-22) oriented  $\text{Al}_{0.5}\text{Ga}_{0.5}\text{N}$  alloy by molecular beam epitaxy. Atomic force microscopy measurements revealed: (i) a one-dimensional ordering tendency along the [1-100] crystallographic direction together with (ii) an in-plane anisotropy of the nanostructure lateral shape with respect to [1-100] and [11-23] crystallographic axes. As a consequence, a morphological transition from dot-shaped islands forming an array of nanochains to wire-shaped objects elongated along the [1-100] direction was evidenced with the increase of the GaN deposited amount. Nanostructures of different dimensionality were fabricated including quantum dots (QDs), quantum wires (QWRs), and quantum wells (QWs), and the excitonic behavior was investigated as a function of the nanostructure shape. The measured temperature dependencies of the exciton radiative decay revealed its direct correlation with a spatial confinement, resulting in a temperature-independent exciton lifetime in the case of QDs, a square root dependence in the case of QWRs, and a linear dependence for QWs. These results, as well as absolute values of measured lifetimes, are in agreement with theoretical predictions.

DOI: [10.1103/PhysRevB.88.125437](https://doi.org/10.1103/PhysRevB.88.125437)

PACS number(s): 72.25.Fe, 73.21.La, 78.55.Cr, 78.67.Hc

**I. INTRODUCTION**

Light matter coupling effects govern functionalities of optoelectronic devices and have multiple applications including solid-state lighting, photodetection, optical communications, and information technologies. Some of these common applications include recording and reading the data stored on an organic support: the information capacity increases with the scaling from compact disks to digital video disks, high-density video disks, and finally blue-ray DVDs with the decrease of the wavelength of compact semiconductor lasers from the near infrared to the deep blue spectral range.<sup>1</sup> Most of these devices are based on stackings of different two-dimensional semiconductor layers with a thickness of the nanometer scale.<sup>2</sup> These stackings are designed in a way to control the light emission wavelengths and output powers as much as possible.<sup>3</sup> An attractive alternative is the use of zero-dimensional objects of nanometer size—quantum dots. Quantum dots have several advantages compared to common two-dimensional layers. First of all, from a technological point of view, the zero-dimension density of state is beneficial for realizing low-threshold operating devices as compared to the three-dimensional and two-dimensional systems.<sup>4</sup> Second, the size and density of these objects may be tuned by changing the growth conditions.<sup>5</sup> Third, these objects having nanometer size are expected to be promising in the field of quantum

optics, for realization of single-photon sources<sup>6</sup> or entangled photon pair emitters.<sup>7</sup> In the specific case of aluminum gallium nitride alloys the devices are aimed to operate in the ultraviolet range of the electromagnetic spectrum. Growth of nitride devices is generally performed along the sixfold symmetry [0001] axis [orthogonal to the (0001) c-plane]. However, the strong pyroelectric polarization and piezoelectric fields that exist along this axis lead to a strong quantum confined Stark effect (QCSE)—a real drawback for optical properties of devices grown along this direction.<sup>8</sup> Alternatively, the growth on nitride planes with high-value Miller indices has been proved to be a possible solution to get rid of QCSE;<sup>9</sup> these so-called semipolar orientations are now a subject of intense investigations.<sup>10</sup> In this work we have restricted our study to the (11-22) semipolar orientation to illustrate the impact of the anisotropy of the growth surface on the morphology and excitonic properties of nano-objects.

The dots investigated here were fabricated by a Stranski-Krastanov (SK) growth.<sup>11,12</sup> This process is classically described by a minimization of the system free energy (defined as the sum of the elastic and surface energies),<sup>13</sup> which can have a strong influence on the nanostructure size and shape.<sup>11</sup> Actually, the shape of these (11-22)-oriented nanostructures is very different from the traditional hexahedral-pyramid shape typical for wurtzite dots grown on polar substrates.<sup>11</sup>

The dots investigated here have an in-plane asymmetry and tend to be aligned along the  $[1-100]$  axis. A remarkable feature of these dots is the continuous transition from: (i) isolated dot-shaped nanostructures (quantum dots, QDs), to (ii) chains of QDs oriented along the  $[1-100]$  axis, and finally (iii) wire-shaped nanostructures (quantum wires, QWRs) as the GaN deposition is increased. Actually, a morphological transition from QDs to QWRs has been reported in several material systems.<sup>13–15</sup> However, little is known about the specific optical properties and quantum physics related to such objects. Therefore, the goal of this work is to couple experimental and theoretical studies of the excitonic behavior in these nanostructures as a function of their morphology. We will show the possibility to trigger the formation of QDs (0D system) or QWRs (one-dimensional or 1D system) by simply engineering the nanostructure morphology during the two- to three-dimensional (2D-3D) growth mode transition.

## II. SAMPLES FABRICATION AND CHARACTERIZATION

The samples have been fabricated as follows: first of all, a 2.2- $\mu\text{m}$ -thick (11-22)-oriented GaN template was grown using metal organic vapor phase epitaxy on a (1-100)-oriented sapphire substrate. The heterostructure itself was grown on that template by molecular beam epitaxy (MBE) as described in Ref. 12. A series of GaN/ $\text{Al}_{0.5}\text{Ga}_{0.5}\text{N}$  active layers, consisting of three planes of GaN nanostructures separated by 30-nm  $\text{Al}_{0.5}\text{Ga}_{0.5}\text{N}$  layers and capped by a GaN layer, have been fabricated. The last layer is deposited for the determination of dot sizes and densities via atomic force microscopy (AFM) experiments. The thickness of GaN layers was varied from 2 to 4.3 nm. It is important to note that the 2D-3D transition is obtained after the deposition of a 2D GaN layer.<sup>12</sup> Furthermore, by controlling the 2D-3D growth mode transition with ammonia (used as the nitrogen source), a sample consisting of three GaN/ $\text{Al}_{0.5}\text{Ga}_{0.5}\text{N}$  quantum wells of 3.7-nm thickness was fabricated.

Figure 1 illustrates the evolution of the dots morphology with the orientation of the  $\text{Al}_{0.5}\text{Ga}_{0.5}\text{N}$  template. In contrast to the typical isotropic shapes of the dots grown on a polar template [Fig. 1(a)], in the case of the semipolar-oriented  $\text{Al}_{0.5}\text{Ga}_{0.5}\text{N}$  template we observe chains of QDs oriented along the  $[1-100]$  direction [Fig. 1(b)]. The thickness of the GaN layer is around 2.4 nm in both samples. In Figs. 1(c) and 1(d), this thickness is increased up to 3.2 nm [Fig. 1(c)] and 4.3 nm [Fig. 1(d)]. As clearly seen, the lateral size of the dots along the  $[1-100]$  direction increases permanently. Strong asymmetry of the grown dots has also been illustrated by the high-resolution transmission electron microscopy (TEM) measurements performed along two crystallographic directions in the dot base. They clearly indicate the formation of

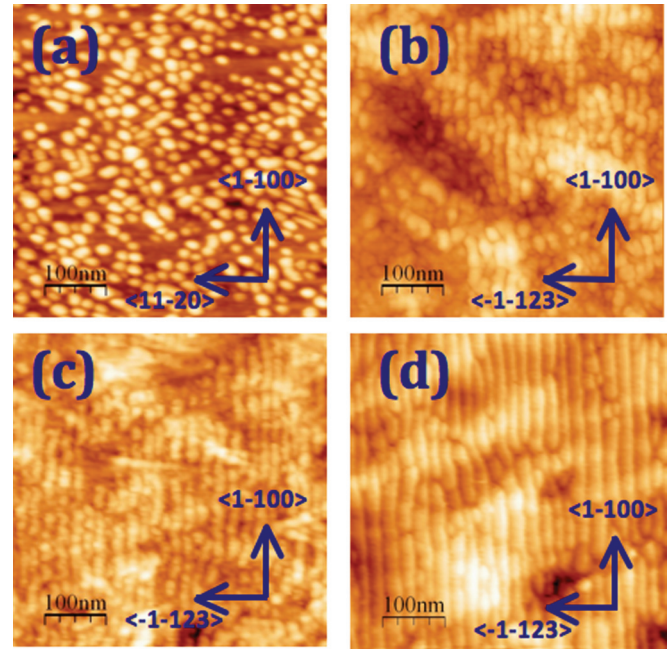


FIG. 1. (Color online) The evolution of the dots morphology with the orientation of the  $\text{Al}_{0.5}\text{Ga}_{0.5}\text{N}$  template. AFM images of GaN dots grown on (0001)-oriented template (a), and GaN nanostructures: dots (b) and wires (c, d), grown on (11-22)-oriented template demonstrating alignment along the  $[1-100]$  direction.

a continuous (undulating) film along the  $[-1-123]$  direction and more efficient coalescence of the dots along the  $[1-100]$  direction.<sup>12</sup> Table I presents the average values of nano-objects as obtained from AFM measurements.

## III. EXPERIMENTAL RESULTS

Time-resolved (TR), time-integrated time-resolved (TITR), and temperature-dependent photoluminescence (PL) experiments have been performed on the samples. To investigate the temperature behavior of the radiative decay of confined excitons, the samples were mounted in a helium flow cryostat, allowing one to vary the temperature from 10 K to 300 K. The laser beam was focused onto the samples to a 100- $\mu\text{m}$ -diameter spot with an average power of 5 mW. The PL was analyzed using a 550-mm monochromator and a CCD camera. A mode-locked frequency-tripled titanium-sapphire laser with a 2-ps pulse width and a wavelength of 260 nm was used as an excitation source. The focused laser spot diameter was also 100  $\mu\text{m}$ . The PL signal was dispersed by an imaging spectrometer and then temporally resolved by a streak camera with an overall time resolution of 8 ps. Figures 2 and 3 illustrate the evolutions of the TITR PL

TABLE I. Lateral sizes and heights of the GaN nanostructures under examination

	4 MLs	6 MLs	9 MLs	12 MLs	16 MLs
$l_{[-1-123]}$ (nm)	$18 \pm 2$	$19 \pm 3$	$20 \pm 4$	$21 \pm 4$	$21 \pm 4$
$l_{[1-100]}$ (nm)	$17 \pm 1$	$25 \pm 5$	$39 \pm 7$	$41 \pm 4$	–
Height (nm)	1.1	$2.3 \pm 0.5$	$2.84 \pm 0.88$	$3.3 \pm 0.6$	$4.31 \pm 0.83$

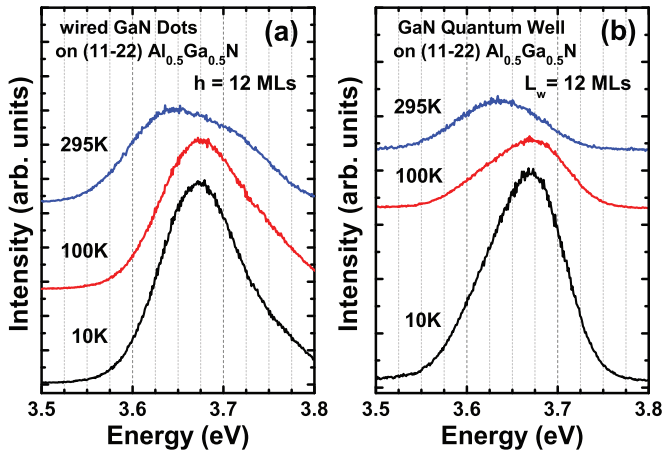


FIG. 2. (Color online) Time-integrated photoluminescence spectra taken for a 12-ML-thick quantum dot sample (a) and for the 12-ML-thick test quantum well (b) at different temperatures.

spectra and peak energies, respectively. Figure 2 depicts the data for 12-monolayer (ML) QD and 12-ML QW samples. The PL peaks are inhomogeneously broadened, which is the result of size and strain distribution in the nano-objects probed by the laser beam.<sup>16</sup> The increase of the broadening with temperature is attributed to interactions with phonons and to the broadening of the thermal distribution of excitons. The ratio of PL intensities at 10 K and 300 K in our experiment is about 2 for the QDs, 10 for QWRs, and 25 for the multiple quantum well, as indicated in Fig. 3(a). In all cases the excitons experience a localization, as evidenced by the low-temperature energy plateaus seen in Fig. 3(b).

The inset in Fig. 3(b) shows the evolution of the transition energy versus the nanostructure size. The apparent saturation of the energy at about 3.6 eV [which is the transition energy we estimate for GaN coherently grown on (11-22) Al<sub>0.5</sub>Ga<sub>0.5</sub>N] indicates a substantial reduction of QCSE in our samples. A rough estimate gives the value of the electric field in the direction orthogonal to the (11-22) plane of approximately 100 kV/cm, as expected from the theoretical calculations.<sup>17-19</sup>

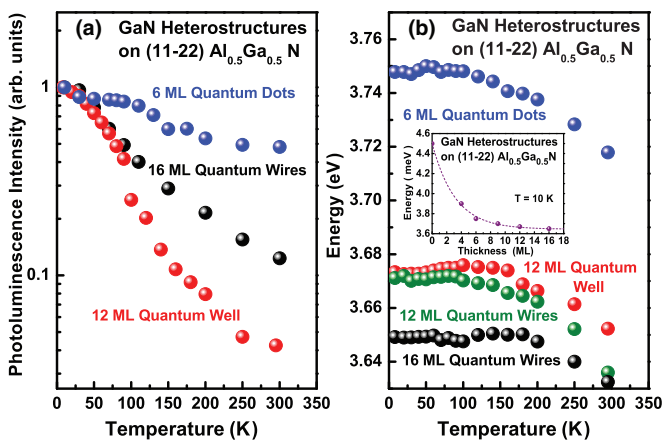


FIG. 3. (Color online) Temperature dependence of the intensity (a) and the energy (b) of the PL peak for different quantum nanostructures. The inset shows the evolution of the energy versus height of the (11-22) nanostructures illustrating the cancellation of the QCSE.

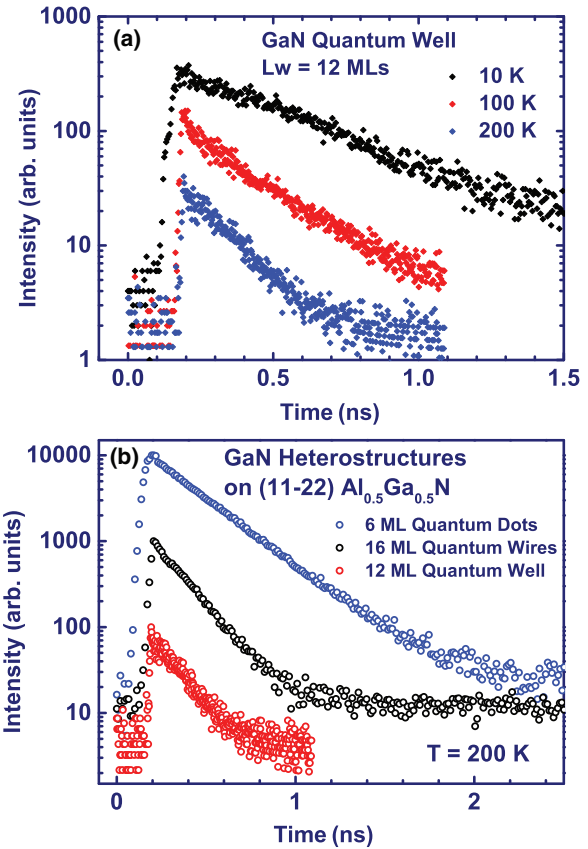


FIG. 4. (Color online) (a) Time-resolved PL spectra recorded for the 12-ML quantum well sample at different temperatures: 10 K (top curve), 100 K (middle curve), and 200 K (bottom curve). (b) Time-resolved PL spectra recorded at 200 K for the 6-ML quantum dot sample (top curve), 16-ML quantum wires sample (middle curve), and 12-ML quantum well samples (bottom curve).

Figure 4(a) illustrates the time evolution of the PL intensity for the 12-ML quantum well sample measured at different temperatures: 10 K, 100 K, and 200 K. The extracted decay times are 480 ps at 10 K, 275 ps at 100 K, 158 ps at 200 K, and 110 ps at room temperature. In contrast with Ref. 20, which reports time-resolved spectra for an A-plane grown GaN-Al<sub>0.13</sub>Ga<sub>0.87</sub>N quantum well, we do not observe here a coexistence of fast and slow decay components. The lack of the fast component (which is usually attributed to the exciton trapping at dislocations) in our spectra is an evidence of lower densities of dislocations and stacking faults in our semipolar GaN/Al<sub>0.5</sub>Ga<sub>0.5</sub>N sample compared to nonpolar A-plane grown quantum wells (in our samples this density is estimated to be in the 10<sup>5</sup> cm<sup>-1</sup> range). Figure 4(b) illustrates the time evolution of the PL intensities for the 6-ML quantum dot sample, the 16-ML quantum wires sample, and 12-ML quantum well samples measured at 200 K. The decay times at 200 K are 271 ps for the 6-ML quantum dot sample, 174 ps for the 16-ML quantum wire sample, and 158 ps for the 12-ML quantum well sample. Previous time-resolved PL studies on GaN self-assembled quantum wires emitting at 4 eV have revealed a two-decay behavior with a fast component at 120 ps and a slower one in the 250-ps range.<sup>21</sup> These values are fully compatible with our measurements: more rapid decay of the

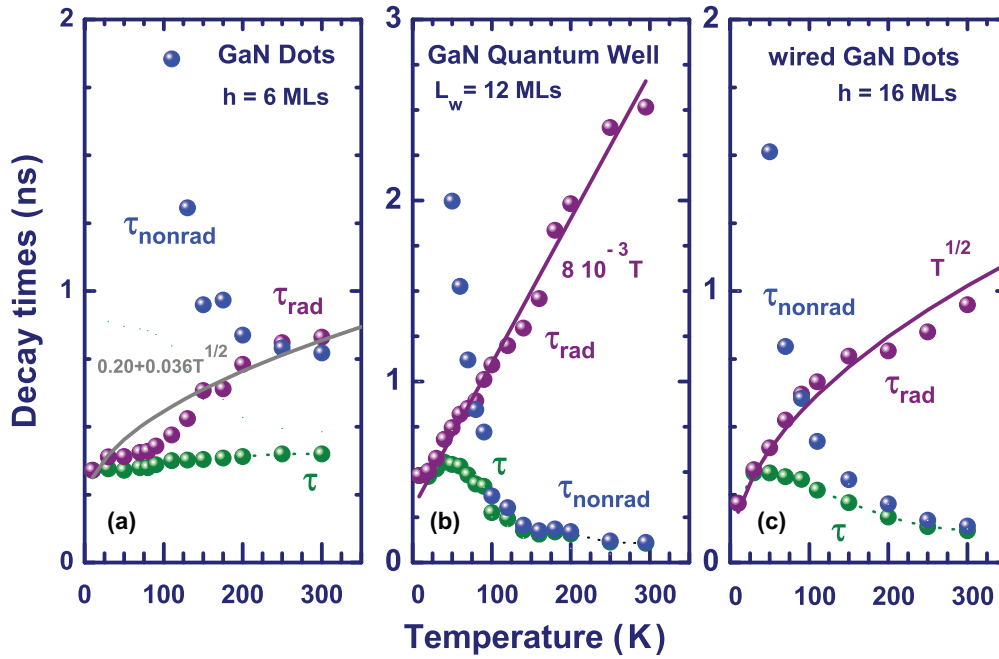


FIG. 5. (Color online) Exciton recombination decay times (green dots), nonradiative components (blue dots), and radiative recombination times (wine dots) for a 6-ML dot sample (a), a 12-ML quantum well sample (b), and a 16-ML wired dot sample (c). Solid lines represent the fit of the data.

fast component in comparison with our samples is related to the higher value of the electron-hole overlap in these quantum wires, while the higher value of decay time for the slow component is attributed to the higher transition energy.

Figures 5(a), 5(b), and 5(c) represent the decay times measured up to room temperature (green dots), calculated values of nonradiative decay times (blue dots), and radiative decay times (wine dots) for typical samples. We have chosen a 6-ML dot sample (a), a 12-ML QW sample (b), and a 16-ML wire sample (c). Following Gurioli *et al.*,<sup>22</sup> the nonradiative  $\tau_{\text{nonrad}}(T)$  and radiative  $\tau_{\text{rad}}(T)$  components of the total decay time  $\tau(T)$  are obtained by the measurement of temperature behaviors of both the PL intensity and the total lifetime. We postulated the low-temperature efficiency of PL to be equal to 1. The evolution of the total, radiative, and nonradiative decay times versus temperature is presented in Fig. 5(a) for the typical semipolar 6-ML QD sample. As expected for the 3D confined excitons, the radiative decay time is constant at low temperatures, with a value of about 300 ps. With increasing temperature it slightly increases as a result of temperature-induced delocalization of the exciton. A similar plot is given in Fig. 5(b) for the 12-ML QW sample. The radiative decay time is equal to 250 ps at 8 K and increases linearly with  $T$  with a slope of 8 ps K<sup>-1</sup>, typical for wurtzite quantum wells [wine-colored line in Fig. 5(b)].<sup>22–26</sup> Figure 5(c) represents the decay times for the 16-ML QWR sample. The radiative decay time increases proportional to  $\sqrt{T}$ , a behavior typical for one-dimensional systems (i.e., excitons confined in a nanowire).<sup>27–29</sup> The fit of the obtained data by a formula  $\tau_{\text{rad}}(T) = c_1 \sqrt{T}$  gives a prefactor  $c_1 = 67 \text{ ps K}^{-1/2}$ . The values of  $c_1$  for GaAs/Al<sub>x</sub>Ga<sub>1-x</sub>As QWRs range between 92 ps K<sup>-1/2</sup> and 200 ps K<sup>-1/2</sup>, depending on the design of the sample, as reported in Refs. 27 and 28. These data correlate

well with the prefactor value measured here for GaN-based QWRs. Finally, we would like to indicate that the deviation of the radiative decay time in the case of the 6-ML sample from a strict constant behavior is indicative of a thermally induced exciton delocalization. As indicated in the figure, it is likely to be fitted by using a square root dependence on  $T$  [ $c_1 = 36 \text{ ps K}^{-1/2}$ , see the gray line in Fig. 5(a)], which is an evidence of the unidimensional delocalization. Interestingly, such a delocalization was not observed for the 4-ML quantum dot sample (not shown here) for which the decay time was constant at 300 ps up to 300 K.

#### IV. DISCUSSION

Figure 5 clearly illustrates the large nonradiative component of the exciton decay. This component is attributed to the existence of various types of dislocations (the density of which in our samples is in the range of  $10^5 \text{ cm}^{-2}$ ) typical for nitride heterostructures (see Refs. 20 and 30). Such dislocations are also present for the (11-22) growth direction, even though its density is lower than in the case of M-plane and A-plane heterostructures.<sup>31</sup>

The theoretical dependence of the exciton radiative lifetime on temperature can be obtained by simply averaging the radiative decay rate of a single exciton with a temperature distribution of exciton states following Boltzmann statistics (see Appendix A for details). Integration through the wave vector space of different dimensions gives the earlier announced dependencies of radiative lifetime:  $\tau \propto T^{3/2}$  for 3D bulk excitons,  $\tau \propto T$  in 2D quantum wells, and  $\tau \propto \sqrt{T}$  in 1D nanowires. For completely localized zero-dimensional excitons in quantum dots,  $\tau$  does not depend on temperature at all. The temperature dependence of the radiative decay time

of one-dimensional excitons reads

$$\tau_{\text{rad}}(T) = c_1 \sqrt{T} = \tau_0^{\text{QWW}} \sqrt{\pi/2} \sqrt{T/T_0}, \quad (1)$$

with  $T_0 = \hbar^2 \omega^2 / (2Mk_B c^2)$ . Here  $\tau_0^{\text{QWW}}$  is the radiative lifetime of a single exciton in a wire,  $\omega$  is the exciton resonance frequency,  $M$  is the translation mass,  $k_B$  is the Boltzmann constant, and  $c$  is the speed of light. We estimate  $T_0 \approx 0.2$  K at  $\hbar\omega = 3.6$  eV. Parameter  $\tau_0$  in a simple model of a strong parabolic lateral confinement reads (details of derivation are given in the Appendix B)

$$\tau_0^{\text{QWW}} = \frac{1}{2\Gamma_0} = \frac{2}{\pi\omega_{\text{LT}}} \frac{c^2 a_w a_e^2 a_h^2}{\varepsilon\omega^2 a_B^3 \bar{a}^4} \exp\left(\frac{\varepsilon\omega^2 \bar{a}^2}{2c^2}\right). \quad (2)$$

Here  $\omega_{\text{LT}}$  is the longitudinal-transverse splitting, and  $a_{e(h)}$  and  $a_w$  are the characteristic lateral sizes of electron (hole) and exciton wave functions, respectively. The parameter  $\bar{a}$  is the average of  $a_e$  and  $a_h$  given by Eq. (B4) in Appendix B, and  $a_B$  is the 3D exciton Bohr radius. In Eq. (2) we set the value of the exponent to unity, thanks to the small value of  $\bar{a} \approx 2$  nm compared to the inverse length of the wave vector of the light in GaN (about  $100 \text{ nm}^{-1}$  at the exciton resonance frequency). For the estimations we can set parameters  $a_e$ ,  $a_h$ , and  $\bar{a}$  equal to the wire radius  $a \approx 2.5$  nm. The characteristic exciton radius in the direction of the wire axis  $a_w$  can be found by a variational calculation (see Appendix B for details). Figure 6 represents the results of this calculation in the range of wire radii  $a$  from 2 to 5 nm. At  $a = 2.5$  nm we obtain  $a_w \approx 5$  nm. At  $\hbar\omega = 3.6$  eV, using  $\hbar\omega_{\text{LT}} = 0.6$  meV,  $\varepsilon = 7$ , and  $a_B = 4$  nm one gets the prefactor  $c_1 \approx 52 \text{ ps K}^{-1/2}$ , in good quantitative agreement with the experimental value of  $67 \text{ ps K}^{-1/2}$ .

The radiative lifetime of a zero-dimensional exciton confined in a QD reads (see Appendix B)

$$\tau_0^{\text{QD}} = \frac{3\hbar c^3}{\omega_{\text{LT}}(\sqrt{\varepsilon}\omega a_B)^3}, \quad (3)$$

and for the same parameters one obtains  $\tau_0^{\text{QD}} \approx 460$  ps, close to the experimentally observed 300 ps.

Let us note that the simple theory on radiative lifetimes of excitons localized in QWRs and QDs serves as a tool for estimating the parameters (such as  $c_1$ ,  $\tau_0^{\text{QWW}}$ ,  $\tau_0^{\text{QD}}$ ) and confirmation of the experimentally observed tendencies. The

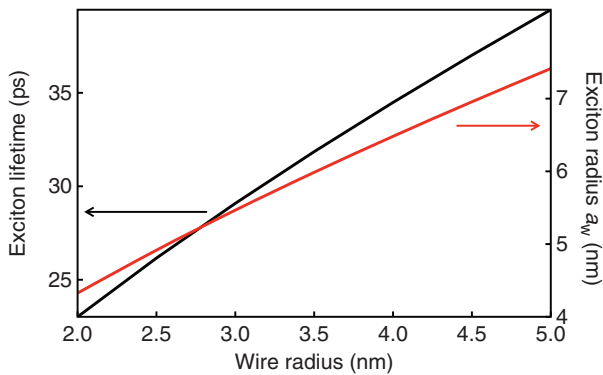


FIG. 6. (Color online) Characteristic exciton radius in the direction of the wire axis and the single-exciton radiative lifetime as a function of the wire radius. The results are obtained through a variational procedure (see Appendix B for details).

more complete models which take into account static and dynamical disorder in QWRs have been published in Refs. 32 and 33. The next order effects [e.g., the dynamical disorder which could originate from a phase separation observed by TEM in the  $\text{Al}_{0.5}\text{Ga}_{0.5}\text{N}$  capping layer (not shown)] can be responsible for the deviations of the experimental data for QWRs from the  $\sqrt{T}$  dependence [see Fig. 5(c)].

To conclude, we have demonstrated the possibility to fabricate QWRs and QDs by taking advantage of a strain-driven epitaxial process leading to a 2D-3D growth mode transition. Using the semipolar (11-22) orientation in the GaN/ $\text{Al}_{0.5}\text{Ga}_{0.5}\text{N}$  material system, arrays of QDs organized in chains along the [1-100] growth plane axis and arrays of QWRs aligned along [1-100] direction are engineered by simply adjusting the GaN deposited thickness. The observation of a zero-dimensional (0D) behavior for the excitons in samples with chains of GaN nanostructures and a one-dimensional (1D) behavior in samples made of arrays of elongated nanostructures agrees well with the theoretical calculations using a confinement potential determined by the specific shape of the nanostructures. Furthermore, the optical data compare well with the range of values measured in other QWR systems, which shows the possibility offered by nitride materials to fabricate heterostructures with either 2D, 1D, or 0D densities of states.

## ACKNOWLEDGMENTS

We acknowledge support from GANEX (ANR-11-LABX-0014). GANEX belongs to the publicly funded “Investissements d’Avenir” program managed by the French ANR agency. This work is partly supported by European Union Grants No. CLERMONT4 PITNGA-2009-235114 and No. INDEX FP7-2011-289968, and the Russian Ministry of Education and Science (Contract No. 11.G34.31.0067). D.R. acknowledges the Ph.D. grant support of ANR “GASIOPE.” M.D. acknowledges financial support from the Dynasty Foundation. The authors are grateful to D. Lefebvre, S. Vezian, P. Vennegues, M. Leroux, N. Kriouche, P. de Mierry, and B. Poulet for their help and fruitful discussions. A. Courville, O. Tottereau, P. Valvin, T. Guillet, and C. Brimont are greatly acknowledged for sample characterization and technical assistance.

## APPENDIX A: TEMPERATURE DEPENDENCE OF EXCITON RADIATIVE LIFETIME FOR DIFFERENT DIMENSIONS

The radiative decay rate  $\Gamma(T)$  of an exciton ensemble can be obtained by averaging those of a single exciton  $\Gamma_0$  over the distribution in  $k$  space. In a simple model where  $\Gamma_0$  is independent of polarization, the total rate is simply a fraction of excitons inside the light cone  $|k| < \omega/c$ . Assuming the Boltzmann statistics for excitons one obtains<sup>23</sup>

$$\Gamma(T) = \Gamma_0 \frac{\int_{|k| < \omega/c} d\mathbf{k} \exp\left(-\frac{\hbar^2 k^2}{2Mk_B T}\right)}{\int d\mathbf{k} \exp\left(-\frac{\hbar^2 k^2}{2Mk_B T}\right)}, \quad (A1)$$

where  $k$  is the wave vector of an exciton center of mass,  $\hbar$  is the Planck constant,  $M$  is the translation mass of an exciton, and

$k_B$  is the Boltzmann constant. The integration in the numerator of (A1) is performed at  $k$  lying inside the light cone, while for the denominator one should integrate over the whole  $k$  space. Let us consider three possible cases with different dimensions of  $k$  space (corresponding to different dimensions of exciton motion), namely, a three-dimensional case (bulk exciton), a two-dimensional case (exciton in a quantum well), and a one-dimensional case (exciton in a quantum wire). For an exciton confined in a quantum dot, due to the absence of free motion the decay is naturally equal to that of a single particle.

### 1. 3D case

Equation (A1) results in

$$\begin{aligned} \Gamma^{\text{bulk}}(T) &= \frac{4}{\sqrt{\pi}} \left( \frac{\hbar^2}{2Mk_B T} \right)^{3/2} \Gamma_0^{\text{bulk}} \\ &\times \int_0^{\omega/c} k^2 dk \exp\left(-\frac{\hbar^2 k^2}{2Mk_B T}\right) \\ &= \Gamma_0^{\text{bulk}} \left[ \text{erf} \sqrt{\frac{T_0}{T}} - \frac{2}{\sqrt{\pi}} \sqrt{\frac{T_0}{T}} \exp\left(-\frac{T_0}{T}\right) \right], \end{aligned} \quad (\text{A2})$$

where  $\text{erf}(x)$  is the error function and  $T_0 = \hbar^2 \omega^2 / (2Mk_B c^2)$ .

The radiative lifetime  $\tau_R^{\text{bulk}} = 1/(2\Gamma^{\text{bulk}})$ . In the region of high temperatures  $T_0/T \ll 1$  one obtains

$$\tau_R^{\text{bulk}}(T) = \frac{3}{4} \sqrt{\pi} \tau_0^{\text{bulk}} \left( \frac{T}{T_0} \right)^{3/2} \propto T^{3/2} \quad (\text{A3})$$

with  $\tau_0^{\text{bulk}} = 1/(2\Gamma_0^{\text{bulk}})$ .

### 2. 2D case

The results for 2D and 1D cases can be obtained in a similar way:

$$\begin{aligned} \Gamma^{\text{QW}}(T) &= \frac{\hbar^2}{Mk_B T} \Gamma_0^{\text{QW}} \int_0^{\omega/c} k dk \exp\left(-\frac{\hbar^2 k^2}{2Mk_B T}\right) \\ &= \Gamma_0^{\text{QW}} \left[ 1 - \exp\left(-\frac{T_0}{T}\right) \right]. \end{aligned} \quad (\text{A4})$$

Radiative lifetime at high temperatures is

$$\tau_R^{\text{QW}}(T) = \tau_0^{\text{QW}} \frac{T}{T_0} \propto T. \quad (\text{A5})$$

### 3. 1D case

For the 1D case,

$$\begin{aligned} \Gamma^{\text{QWW}}(T) &= \left( \frac{\hbar^2}{2\pi Mk_B T} \right)^{1/2} \Gamma_0^{\text{QWW}} \\ &\times \int_{-\omega/c}^{\omega/c} dk \exp\left(-\frac{\hbar^2 k^2}{2Mk_B T}\right) \\ &= \Gamma_0^{\text{QWW}} \text{erf} \sqrt{\frac{T_0}{T}}. \end{aligned} \quad (\text{A6})$$

The radiative lifetime at high temperatures is

$$\tau_R^{\text{QWW}}(T) = \frac{\sqrt{\pi}}{2} \tau_0^{\text{QWW}} \sqrt{\frac{T}{T_0}} \propto \sqrt{T}. \quad (\text{A7})$$

## APPENDIX B: SINGLE-EXCITON RADIATIVE DECAY IN NANOWIRES AND DOTS

Let us now focus on the calculation of single-exciton decay times  $\tau_0 = 1/(2\Gamma_0)$  in nanowires and quantum dots.

### 1. Quantum dot

Let us consider a quantum dot with a strong confinement in all spacial directions (i.e., the separation between energy levels due to confinement is larger than the Coulomb energy). The conventional way to derive radiative decays of excitons in different nanostructures is a nonlocal dielectric response approach.<sup>34</sup>  $\Gamma_0^{\text{QD}}$  is obtained by taking the overlap between a 3D Green function and the exciton wave function  $\Phi(\mathbf{r})$  at coinciding electron and hole coordinates,

$$\Gamma_0^{\text{QD}} = \frac{1}{6} q^2 a_B^3 \omega_{\text{LT}} \iint d\mathbf{r} d\mathbf{r}' \frac{\sin q|\mathbf{r} - \mathbf{r}'|}{|\mathbf{r} - \mathbf{r}'|} \Phi(\mathbf{r}) \Phi(\mathbf{r}'), \quad (\text{B1})$$

where  $q$  is the light wave vector in quantum dot material,  $a_B$  is the 3D exciton Bohr radius, and  $\omega_{\text{LT}}$  is the longitudinal-transverse splitting. To simplify, let us consider a spherical dot with parabolic confinement and effective radii  $a_{e,h}$  for electron and hole. Then  $\Phi(\mathbf{r})$  reads

$$\Phi(\mathbf{r}) = \frac{1}{\pi^{3/2} (a_e a_h)^{3/2}} \exp\left(-\frac{r_e^2}{2a_e^2}\right) \exp\left(-\frac{r_h^2}{2a_h^2}\right). \quad (\text{B2})$$

The integral in Eq. (B1) can be calculated analytically and gives

$$\Gamma_0^{\text{QD}} = \frac{1}{6} \omega_{\text{LT}} (q a_B)^3 \frac{\bar{a}^6}{a_e^3 a_h^3} \exp(-q^2 \bar{a}^2), \quad (\text{B3})$$

where

$$\bar{a}^2 = \frac{2a_e^2 a_h^2}{a_e^2 + a_h^2}. \quad (\text{B4})$$

For  $a_e = a_h$  and  $q\bar{a} \ll 1$  the dependence on the dot size vanishes, yielding

$$\Gamma_0^{\text{QD}} = \frac{1}{6} \omega_{\text{LT}} (q a_B)^3. \quad (\text{B5})$$

### 2. Quantum wire

Let us consider a cylindrical quantum wire of radius  $a$  with a strong lateral confinement. The Hamiltonian of the internal motion of exciton in  $z$  direction reads

$$\mathcal{H}_z = -\frac{\hbar^2}{2\mu_{eh}} \frac{\partial^2}{\partial z^2} - \frac{e^2}{\kappa \sqrt{z^2 + d^2}}, \quad (\text{B6})$$

where  $z = z_e - z_h$ . The parameter  $d$  is introduced to eliminate the energy divergency arising in the one-dimensional Coulombic problem.<sup>35</sup> For simplicity we will take  $d = a$ . The wave function of the Hamiltonian (B6) can be found using a variational technique with the trial function  $f(z)$  written as follows:<sup>36</sup>

$$f(z) = \frac{1}{\sqrt{a_w}} \exp\left(-\frac{|z|}{a_w}\right), \quad (\text{B7})$$

with a single variational parameter  $a_w$ . The results of variational calculations for  $a_w$  are presented in Fig. 6.  $\Gamma_0^{\text{QWW}}$  is

given by<sup>34</sup>

$$\Gamma_0^{\text{QWW}} = \frac{\pi}{4} a_B^3 q^2 \omega_{\text{LT}} \iint d\rho d\rho' \Phi(\rho) \Phi(\rho') J_0(q|\rho - \rho'|), \quad (\text{B8})$$

with  $J_0$  being the Bessel function of zero index and the following wave function:

$$\Phi(\rho) = \frac{1}{\pi \sqrt{a_w a_e a_h}} \exp\left(-\frac{\rho^2}{\bar{a}^2}\right), \quad (\text{B9})$$

where  $a_e$  and  $a_h$  are in-plane effective radii of the electron and hole and  $\bar{a}$  is defined in Eq. (B4). The integration gives

$$\Gamma_0^{\text{QWW}} = \frac{\pi}{4} \omega_{\text{LT}} \frac{q^2 a_B^3 \bar{a}^4}{a_w a_e^2 a_h^2} \exp\left(-\frac{1}{2} q^2 \bar{a}^2\right). \quad (\text{B10})$$

For  $a_e = a_h$ ,  $q\bar{a} \ll 1$ , and GaN parameters we obtain the results on nanowire lifetimes presented in Fig. 6. One can see that the values of  $\tau_0^{\text{QWW}}$  are more than 1 order of magnitude less than those of  $\tau_0^{\text{QW}}$ .

<sup>1</sup>Piprek, *Nitride Semiconductor Devices: Principles and Simulation* (Wiley, New York, 2007).

<sup>2</sup>S. Nakamura and S. Chichibu, *Introduction to Nitride Semiconductor Blue Lasers and Light Emitting Diodes* (Taylor and Francis, London, 2000).

<sup>3</sup>R. Chen, T.-T. D. Tran, K. W. Ng, W. S. Ko, L. C. Chuang, F. G. Sedgwick, and C. Chang-Hasnain, *Nat. Photonics* **5**, 170 (2011).

<sup>4</sup>D. Bimberg, M. Grundman, and N. Ledentsov, *Quantum Dot Heterostructures* (Wiley, New York, 1998).

<sup>5</sup>K. Hoshino, S. Kako, and Y. Arakawa, *Appl. Phys. Lett.* **85**, 1262 (2004).

<sup>6</sup>C. Santori, S. Götzinger, Y. Yamamoto, S. Kako, K. Hoshino, and Y. Arakawa, *Appl. Phys. Lett.* **87**, 051916 (2005).

<sup>7</sup>N. Akopian, N. H. Lindner, E. Poem, Y. Berlatzky, J. Avron, D. Gershoni, B. D. Gerardot, and P. M. Petroff, *Phys. Rev. Lett.* **96**, 130501 (2006).

<sup>8</sup>J. S. Im, H. Kollmer, J. Off, A. Sohmer, F. Scholz, and A. Hangleiter, *Phys. Rev. B* **57**, R9435 (1998).

<sup>9</sup>P. Waltereit, O. Brandt, A. Trampert, H. Grahn, J. Menninger, M. Ramsteiner, M. Reiche, and K. Ploog, *Nature (London)* **406**, 865 (2000).

<sup>10</sup>H. Masui, S. Nakamura, S. P. DenBaars, and U. K. Mishra, *IEEE Trans. Electron Devices* **57**, 88 (2010).

<sup>11</sup>J. Brault, T. Huault, F. Natali, B. Damilano, D. Lefebvre, M. Leroux, M. Korytov, and J. Massies, *J. Appl. Phys.* **105**, 033519 (2009).

<sup>12</sup>A. Kahouli, N. Kriouche, J. Brault, B. Damilano, P. Vennéguès, P. de Mierry, M. Leroux, A. Courville, O. Tottreau, and J. Massies, *J. Appl. Phys.* **110**, 084318 (2011).

<sup>13</sup>J. Tersoff and R. M. Tromp, *Phys. Rev. Lett.* **70**, 2782 (1993).

<sup>14</sup>J. Brault, M. Gendry, G. Grenet, G. Hollinger, J. Olivares, B. Salem, T. Benyattou, and G. Bremond, *J. Appl. Phys.* **92**, 506 (2002).

<sup>15</sup>B. Amstatt, J. Renard, C. Bougerol, E. Bellet-Amalric, B. Gayral, and B. Daudin, *Phys. Rev. B* **79**, 035313 (2009).

<sup>16</sup>J. Y. Marzin, J. M. Gérard, A. Izraël, D. Barrier, and G. Bastard, *Phys. Rev. Lett.* **73**, 716 (1994).

<sup>17</sup>T. Takeuchi, H. Amano, and I. Akasaki, *Jpn. J. Appl. Phys.* **39**, 413 (2000).

<sup>18</sup>A. E. Romanov, T. J. Baker, S. Nakamura, J. S. Speck, and E. U. Group (ERATO/JST UCSB Group), *J. Appl. Phys.* **100**, 023522 (2006).

<sup>19</sup>P. Bigenwald, B. Gil, F. Benharrats, K. Zitouni, and A. Kadri, *Semicond. Sci. Technol.* **27**, 024009 (2012).

<sup>20</sup>P. Corffdir, P. Lefebvre, L. Balet, S. Sonderegger, A. Dussaigne, T. Zhu, D. Martin, J.-D. Ganière, N. Grandjean, and B. Deveaud-Plédran, *J. Appl. Phys.* **107**, 043524 (2010).

<sup>21</sup>J. Arbiol, C. Magen, P. Becker, G. Jacopin, A. Chernikov, S. Schäfer, F. Furtmayr, M. Tchernycheva, L. Rigutti, J. Teubert, *et al.*, *Nanoscale* **4**, 7517 (2012).

<sup>22</sup>M. Gurioli, A. Vinattieri, M. Colocci, C. Deparis, J. Massies, G. Neu, A. Bosacchi, and S. Franchi, *Phys. Rev. B* **44**, 3115 (1991).

<sup>23</sup>J. Feldmann, G. Peter, E. O. Göbel, P. Dawson, K. Moore, C. Foxon, and R. J. Elliott, *Phys. Rev. Lett.* **59**, 2337 (1987).

<sup>24</sup>M. Colocci, M. Gurioli, A. Vinattieri, F. Fermi, C. Deparis, J. Massies, and G. Neu, *Europhys. Lett.* **12**, 417 (1990).

<sup>25</sup>P. Lefebvre, J. Allègre, B. Gil, A. Kavokine, H. Mathieu, W. Kim, A. Salvador, A. Botchkarev, and H. Morkoc, *Phys. Rev. B* **57**, R9447 (1998).

<sup>26</sup>L. Béaur, T. Bretagnon, B. Gil, A. Kavokin, T. Guillet, C. Brimont, D. Tainoff, M. Teisseire, and J.-M. Chauveau, *Phys. Rev. B* **84**, 165312 (2011).

<sup>27</sup>D. S. Citrin, *Phys. Rev. Lett.* **69**, 3393 (1992).

<sup>28</sup>H. Akiyama, S. Koshihata, T. Someya, K. Wada, H. Noge, Y. Nakamura, T. Inoshita, A. Shimizu, and H. Sakaki, *Phys. Rev. Lett.* **72**, 924 (1994).

<sup>29</sup>D. Gershoni, M. Katz, W. Wegscheider, L. N. Pfeiffer, R. A. Logan, and K. West, *Phys. Rev. B* **50**, 8930 (1994).

<sup>30</sup>Z. H. Wu, A. M. Fischer, F. A. Ponce, B. Bastek, J. Christen, T. Wernicke, M. Weyers, and M. Kneissl, *Appl. Phys. Lett.* **92**, 171904 (2008).

<sup>31</sup>A. Dadgar, R. Ravash, P. Veit, G. Schmidt, M. Müller, A. Dempewolf, F. Bertram, M. Wieneke, J. Christen, and A. Krost, *Appl. Phys. Lett.* **99**, 021905 (2011).

<sup>32</sup>D. Y. Oberli, M.-A. Dupertuis, F. Reinhardt, and E. Kapon, *Phys. Rev. B* **59**, 2910 (1999).

<sup>33</sup>T. Guillet, R. Grousson, V. Voliotis, X. L. Wang, and M. Ogura, *Phys. Rev. B* **68**, 045319 (2003).

<sup>34</sup>E. L. Ivchenko and A. V. Kavokin, *Sov. Phys. Solid State* **34**, 968 (1992).

<sup>35</sup>J. Javanainen, J. H. Eberly, and Q. Su, *Phys. Rev. A* **38**, 3430 (1988).

<sup>36</sup>M. Degani and O. Hipólito, *Phys. Rev. B* **35**, 9345 (1987).